

Development of structure within the turbulent wake of a porous body. Part 2. Evolution of the three-dimensional features

By Z. HUANG, J. G. KAWALL AND J. F. KEFFER

Department of Mechanical Engineering, University of Toronto, Toronto, Ontario,
Canada M5S 1A4

(Received 15 January 1995 and in revised form 16 June 1996)

The present investigation deals with the development stage ($x/d = 20\text{--}100$) of the porous-body wake, generated by a mesh strip. Pattern-recognition analysis was applied to the velocity signals from hot-wire measurements in the vertical centreplane and various horizontal planes in the flow field. Spanwise coherent structures (with ω_z) and lateral coherent structures (ω_y) have been identified. An examination of the fine-scale turbulence is used to show that the two kinds of structures are indeed connected. In the near region of the wake, the lateral structures are ‘ribs’ attached to the spanwise vortices. In the intermediate region, the interaction of the two structures changes the original spanwise vortices into three-dimensional structures. Beyond this zone, in the far region, the ‘legs’ of the original spanwise structure merge with the ‘ribs’, and it can be inferred that the coherent structures within the flow are essentially randomly distributed hairpin-like vortices.

1. Introduction

In recent years, there has been a considerable amount of research on the coherent structures within the near and far regions of plane turbulent wake flows. In terms of the principal vorticity axes, attention has been concentrated on spanwise (ω_z) vortices and lateral (ω_y) vortices. The predominant feature of the near-wake region is the quasi-periodic Kármán vortex street, with distinct spanwise vorticity (ω_z). In the far-wake region, where the flow is fully developed, the coherent motions have been described in terms of spanwise and lateral vortices. The spanwise vortices in this region are organized motions with a dominant vorticity component in the spanwise (or z) direction, resembling the Kármán vortices in the near wake but of larger scale and less organized. These motions are referred to as ‘secondary structures’ by Cimbalá, Nagib & Roshko (1988). The lateral vortices, sometimes referred to as ‘rollers’, have vorticity axes roughly perpendicular to the spanwise direction and approximately aligned in the principal direction of mean strain. Thus, the occurrence of these structures is indicated by a significant coherent vorticity in the lateral direction, i.e. ω_y . Ferré & Giralt (1989) found that these rollers tend to occur as pairs of counter-rotating vortices, with backward flow between them.

Much has been uncovered about the coherent structures in turbulent wake flows. However, little is known about the possible relation between the spanwise and lateral structures in a given region of the flow, although some speculation exists in the literature (e.g. Hayakawa & Hussain 1989; Ferré *et al.* 1990; Antonia *et al.* 1987). We also note (Hayakawa & Hussain 1989) that one must be careful to discriminate

between the lateral vorticity (ω_y) due to ‘ribs’ and that due to the ‘legs’ of hairpin structures. Recently, Zhou & Antonia (1993) studied the relationship between critical points in the vertical and horizontal planes of a near wake. Their results show that in the near-wake region, foci in the horizontal (x, z)-plane mostly occur with the saddles in the vertical (x, y)-plane. This indicates that vortices found in the horizontal planes correspond to rib-like structures. It should be noted however, that critical points in the flow may be caused by small-scale motions and these do not necessarily correspond to the centre of a large-scale motion.

This paper deals with the experimental study of a plane turbulent wake generated by a mesh strip, with the aim of providing information on the relationship between the above-mentioned two types of coherent motions.

2. Experimental details

2.1. Velocity measurement

The experimental set-up is described in the Part 1 of the present paper (Huang & Keffer 1996). The wakes were generated by means of a mesh-strip with a solidity of 60%. The mesh strip was made of stainless-steel wire screen, which has 24×24 wires per square inch and a wire diameter of 0.38 mm. The Reynolds number based on the wire diameter is 230. The width (d) of the wake generator was 18 mm and the length (L), 0.91 m, giving an aspect ratio (L/d) of approximately 50. A free-stream velocity (U_0) of 10.2 m s^{-1} was used, so that the Reynolds number based on d was about 11000.

Multi-point measurements were taken in the vertical centreplane of the flow with a rake of eight X-wire probes, which responded to the U - and V -signals, and in various horizontal planes with a rake of eight X-wire probes, which responded to the streamwise and spanwise (U and W) signals. Each signal was low-pass filtered at 2 kHz and digitized at a rate of 6250 points per second by means of a 12-bit A/D converter. The length of each signal processed was approximate 40 s. A Cartesian coordinate system was employed, with x in the streamwise or U -direction, y in the lateral or V -direction and z in the spanwise or W -direction, parallel to the wake generator. Measurements were taken at various streamwise positions from $20d$ to $100d$. The y -positions for the horizontal-plane measurements were taken at the approximate maximum shear positions of the flow. The probe spacing of the rake was 8 mm for the measurements before $x = 50d$, and 16 mm at and beyond $x = 50d$. A definition sketch of the flow is shown in figure 1.

2.2. Pattern-recognition analysis and fine-scale activity indicator function

In the present investigation, the velocity data obtained in the porous-body wake were analysed by means of a modified version of the pattern-recognition technique, described by Ferré & Giralt (1989). This technique is designed to extract repetitive trends or patterns embedded in multi-point digital turbulent signals. With the aid of appropriate software, correlations between a prescribed pattern or template and a given set of measured multi-point signals are computed. These correlations are assessed statistically and an ensemble of individual realizations of a repetitive pattern is obtained. An ensemble-averaged pattern is then determined. In general, the results can be improved through an iteration process in which the signals are re-analysed with the central portion of the current ensemble-averaged pattern being used as the template.

In the vertical plane, the velocity signals are presented as a summation of the averaged (structure) convection velocity, coherent components (u_c) and incoherent components [$U(i) = U_c + u_c(i) + u_r(i)$]. Thus, the fluctuating component of the velocities

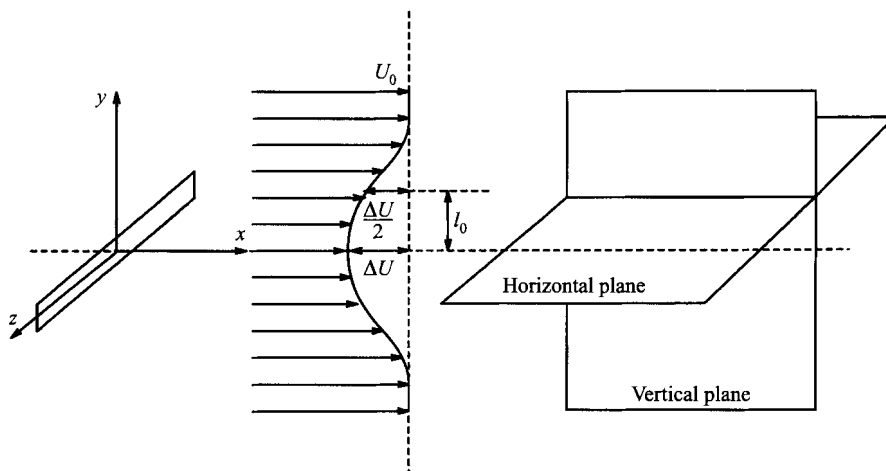


FIGURE 1. Definition sketch.

is expressed as $u = u_c + u_r$. At each specific streamwise location, U_c is selected, based on a trial-and-error pattern-recognition procedure. This generates a result such that the centre of rotation from the ensemble-averaged velocity vectors coincides with the centre of the vorticity contours. It has been found that U_c selected through such a criterion also enables the pattern recognition procedure to identify the maximum number of realizations. In the horizontal plane, the averaged velocity in the measuring plane is used in place of U_c .

With the pattern-recognition analysis, the results from multiple iterations will always converge to the dominant mechanism in the flow, regardless of the initial template. However, in turbulent flows, there may exist more than one mode of coherent motions. In the present experiment, both single- and multiple-iteration analyses were performed for each situation. The results from these two analyses were then checked against each other. With the first iteration of the pattern-recognition analysis, the secondary structures can be identified. This is performed with a trial-and-error method that uses a variety of initial templates. The statistical data ensure that the resulting patterns represent significant portions of the flow. With this method, lateral structures are also identified in the near-wake region, as can be seen later in §4. In most cases we present the ultimate (dominant) velocity patterns, except for the lateral structures in the near region, where the first iteration is presented. This represents a secondary structure in the flow. Statistics presented in §§3.3 and 4.2 are based on the results from the first iteration. The U_c are based upon multiple iterations.

In the near-wake region of the flow, the measurement probes were 8 mm apart, and the rake covered the whole wake adequately. Pattern-recognition analysis, as described previously, was performed on the measured data. In the intermediate and far regions, where the scales of coherent motions are larger than they are in the near wake, the probe spacing was doubled to 16 mm, and an 'interpolated' pattern-recognition analysis was performed, in order to portray the large-scale structures with the same resolution as in the near wake. In the vertical plane, this analysis is performed with data taken from two or more separate measurements of velocity signals. The rake was initially mounted at the lowest position for the first measurement, and was then moved upward progressively by 8 mm for the other measurement(s). For each measurement, a specific template was generated that simulates a common vortex pattern but with different centre positions (with 8 mm difference in the y -direction). Pattern-recognition

analysis was then performed with that template. The objective of this series of analyses was to identify, from different measurements, the repetitively occurring velocity realizations due to the same coherent structures. By rearranging the ensemble-averaged data according to their physical positions, one can combine the results from these measurements and generate a smooth outcome, as illustrated in §3.1. With respect to the horizontal plane, where coherent structures do not have any preferred spanwise location, the ‘interpolated’ analysis was performed with a single measurement of a set of velocity signals. The interpolated analysis for this plane involves two pattern-recognition operations. These are based on two different templates that have the same pattern but with the centres 8 mm apart (in the frame). This simulates two separate measurements taken within the same horizontal plane, at two spanwise positions that are 8 mm apart.

A fine-scale turbulence activity indicator function was used to investigate the relationship between the fine-scale turbulent motions and the large-scale organized structures within the wake. This function, which is defined as the averaged envelope of the temporal second derivatives of the (u and v) or (u and w) turbulent signals, is highly sensitive to the high-frequency components of the signals but is effectively insensitive to the footprints of the large-scale coherent structures within a flow. Thus, it proves an instantaneous measure of the effect of the fine-scale (random) turbulent motions at specified locations in a flow. It should be noted that unlike the intermittency function, this fine-scale turbulence indicator function does not involve a threshold level. It is a real-time function for each probe and can be ensemble-averaged in the same way as the velocity signals. Details concerning the determination of this function have been reported by Ferré *et al.* (1990).

The sectional streamlines, hereafter referred to simply as the streamlines, are defined by

$$\frac{dx}{u} = \frac{dy}{v}$$

for the vertical plane, or

$$\frac{dx}{u} = \frac{dz}{w}$$

for the horizontal plane. In the present research, the lines are calculated by numerically integrating one of the above equations. In theory, a streamline which begins within a picture frame (flow field) will either lead to the outside of the picture or approach, as its limit, a critical point within the field. In the numerical computation, the streamlines are terminated when they reach the boundary of the computational domain or when the integration reaches an upper limit that restricts the length of the streamlines.

3. Evolution of spanwise structures

X-wire anemometry measurements were taken at various streamwise positions in the vertical (x, y) centreplane of the flow. The initial template used in the pattern-recognition analysis of the u - and v -signals measured with the rake is presented in figure 2. This particular template was selected in order to identify the ‘footprints’ of two-dimensional vortices and was generated by means of a numerical procedure, similar to that used by Giralt & Ferré (1993), in which the passage of a single vortex across a vertical rake of X-wire probes was simulated. It should be emphasized that even if different temperatures are used, the pattern-recognition analysis will still detect the same dominant structures in the flow.

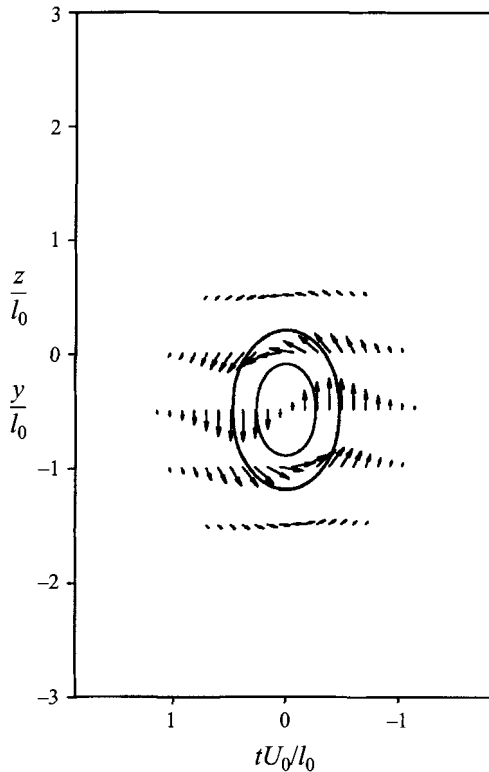


FIGURE 2. Single-roller template used for the pattern-recognition analysis.

3.1. Ensemble-averaged velocities

The ensemble-averaged velocity vector 'map' resulting from the pattern-recognition analysis pertaining to the streamwise position at $24d$ is presented in figure 3(a), superimposed on the corresponding streamlines. This position is the streamwise location at which the periodicity of the flow is most prominent. Corresponding results for $50d$ and $100d$ are presented in figures 3(b) and 3(c) respectively. In these figures, l_0 represents the half-width of the wake (see figure 3(c) at the streamwise position of $24d$, U_0 denotes the free-stream velocity and t represents time. For the purpose of illustration, the pattern of streamlines calculated from the velocity vectors is superimposed. (Since the horizontal and vertical scales in the figure are not the same, the vector do not appear to be exactly tangent to the streamlines in the figure.) Taylor's 'frozen-turbulence' hypothesis (i.e. $\Delta x = -U_0 \Delta t$, where Δx is a streamwise distance travelled in a time Δt) was used in the presentation of these results, so that the temporal footprints of the large-scale coherent structures within the flow could be interpreted in a spatial fashion. It may be remarked that, for the velocity and fine-scale indicator function, the use of Taylor's hypothesis is for the purpose of presentation, and does not necessarily require explicit conversion of the time coordinates of signals into streamwise coordinates. In addition, since the convection velocity U_c and the half-width of the wake l_1 are functions of streamwise position x , the constant velocity U_0 and the width l_0 are used in the coordinate system.

Figures 3(a) and 3(b) both indicate that alternating, counter-rotating, quasi-periodic and predominantly spanwise vortices are present in the flow. The counter-clockwise rotation depicted in the centre ($tU_0/l_0 = 0$) of the figures represents the central structures determined directly with the aid of the template shown in figure 2. The clock-

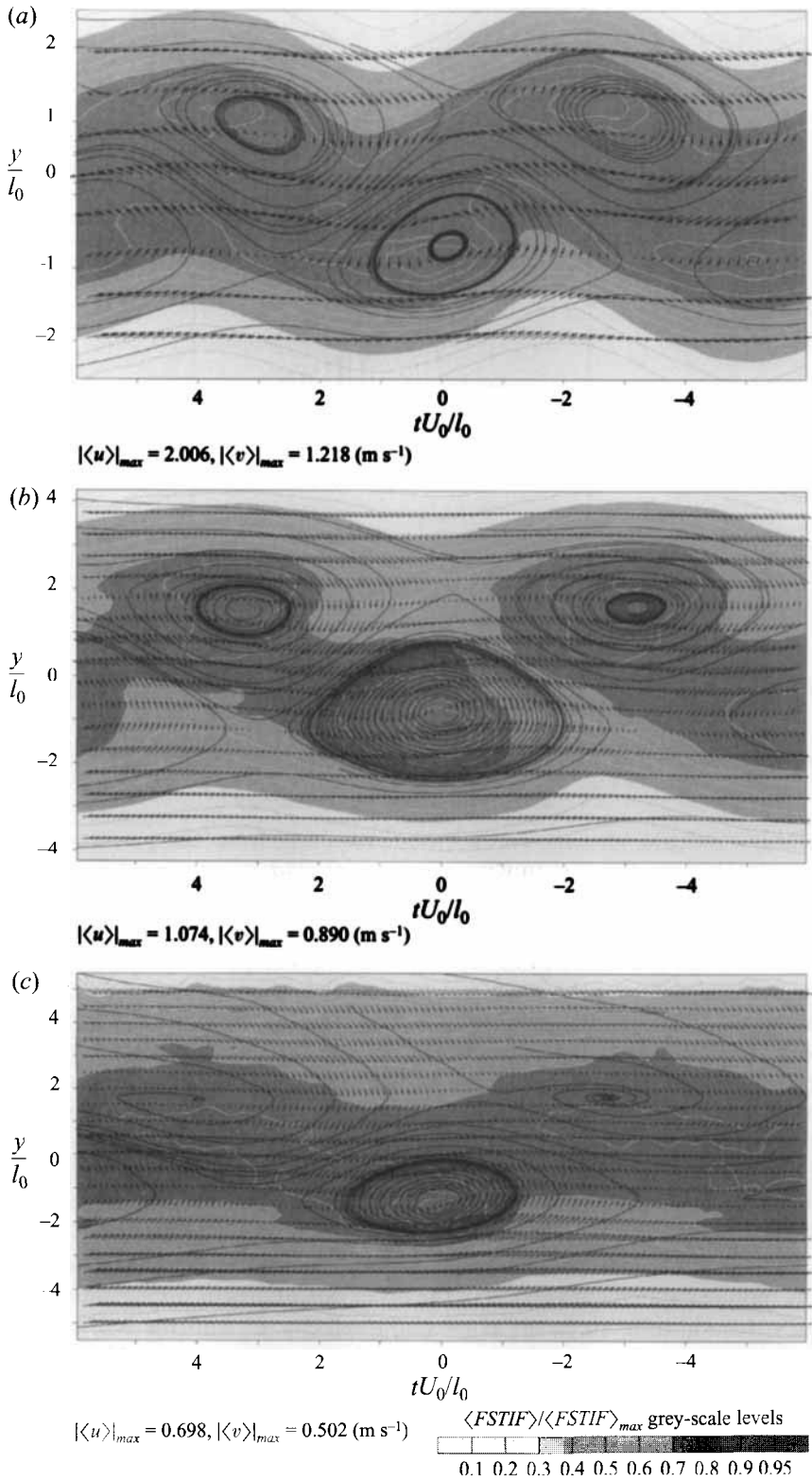


FIGURE 3. For caption see facing page.

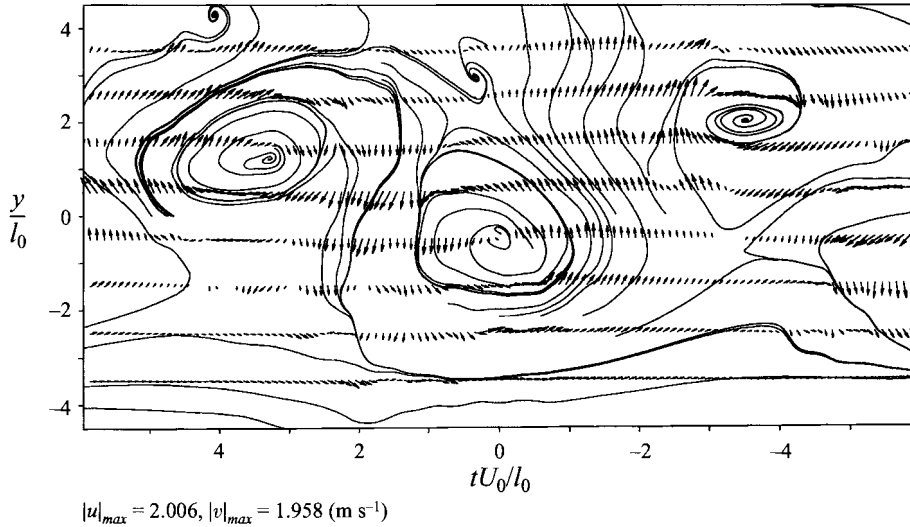


FIGURE 4. ‘Instantaneous’ u - and v -velocity vectors and streamline patterns at $x = 50d$.

wise rotation before and after the central structure is due to the quasi-periodic occurrence of the alternate vortices. The ratio of the lateral spacing between these vortices, Δh , and the streamwise spacing, Δx , is about 0.3, which is close to the $\Delta h/\Delta x$ ratio of 0.281 for a Kármán vortex street.

Downstream of $x \approx 50d$, the spanwise structures in the flow start to lose their periodicity, as is evident from figure 3(c). Consequently, at $x = 100d$ in the far wake, the velocity vectors associated with the clockwise rotation have become less significant. The ‘instantaneous’ pattern of the flow is presented in figure 4.

The ω_z -vorticity iso-contours corresponding to the velocity maps in figures 3(a–c) are presented in figures 5(a–c), respectively. The vorticity is defined as

$$\omega_z \approx -\frac{1}{U_c} \frac{\Delta v_c}{\Delta t} - \frac{\Delta u_c}{\Delta y},$$

where U_c is the convection velocity. The iso-contour lines in these figures represent values equal to $\pm 10\%$, $\pm 25\%$, $\pm 50\%$ and $\pm 75\%$ of the peak vorticity. The arrowheads in the figures indicate the sign and relative magnitude of the quantity. Figure 5(a) confirms that the large-scale spanwise structures in the near region ($24d$) are essentially quasi-periodic vortices that occur alternately above and below the horizontal centreplane of the flow. It also shows that a small amount of vorticity is distributed between vortex cores with the same sense of rotation, with the 10% vorticity iso-contours enveloping the cores on each side of the wake. This seems to be a peculiar feature of the porous-body wake. In the intermediate region, as is shown in figure 5(b) (for $x = 50d$), the vorticity between the adjacent vortex cores becomes negligible, and the 10% contour lines form closed loops. Although the streamwise spacing (Δx) of the vortices is about the same as in the near region, the lateral spacing (Δh) becomes larger. In the far region, very little evidence of periodicity can be discerned in the vorticity contours (figure 5c, $x = 100d$).

The results for the porous-body wake indicate that the coherent structures in this

FIGURE 3. Ensemble-averaged u - and v -velocity vectors superimposed on the grey-scale iso-contours of the fine-scale indicator function (FSTIF): (a) in the near region, $x/d = 24$; (b) in the intermediate region, $x/d = 50$; (c) in the far region, $x/d = 100$.

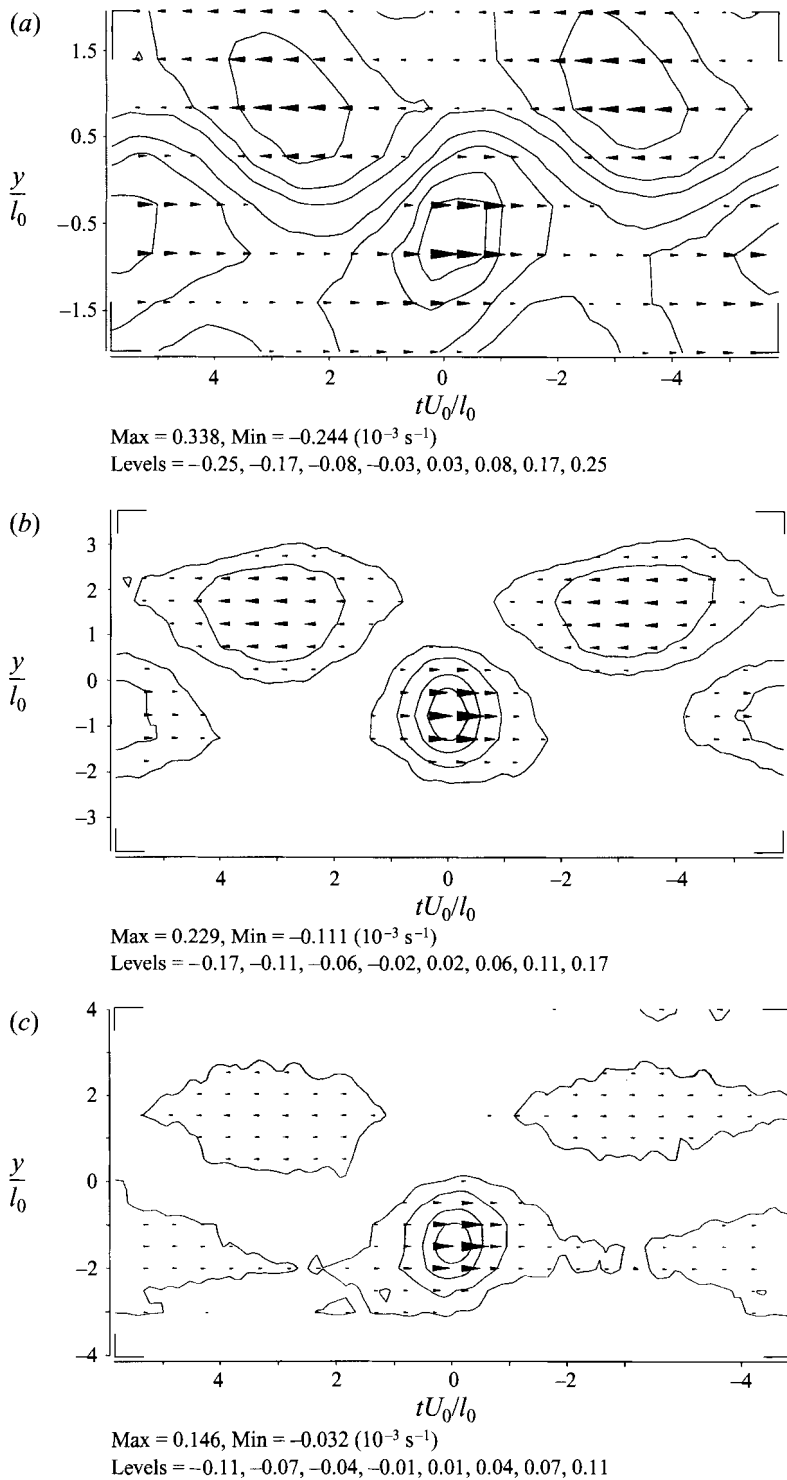


FIGURE 5. Coherent ω_z -vorticity iso-contours in (a) the near region, $x/d = 24$; (b) in the intermediate region, $x/d = 50$; (c) in the far region, $x/d = 100$.

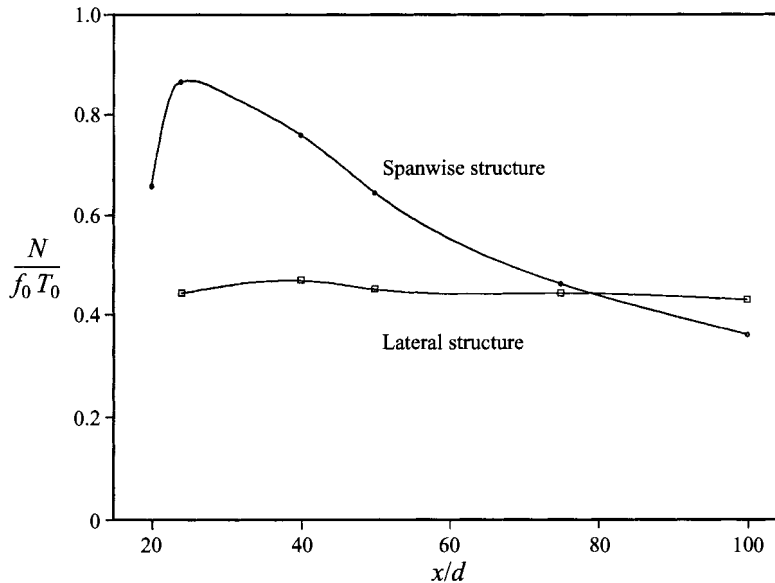


FIGURE 6. Number of spanwise and lateral vortices identified by the single-roller template.

flow are qualitatively similar to those in a solid-body wake. But the detailed characteristics of the two flows are still different. In the case of the solid-body wake, the Kármán structures result from the direct roll-up of the boundary layer fluid that separates from the solid wake generator. These structures grow rapidly and become periodic with an essentially constant characteristic frequency in the very early stages of the wake development. In contrast, for the case of the porous-body wake, the Kármán-like structures are due to the relatively gradual merging and interaction of the small-scale vortices originating at the two edges of the porous wake generator (Huang & Keffer 1996).

3.2. Fine-scale turbulence activity and entrainment

Figure 3 also shows a grey-scale x - y map of the ensemble (or phase)-averaged fine-scale turbulence indicator function (FSTIF) in near region of the wake ($24d$). This map shows the action of the fine-scale turbulent motions, superimposed on the similarly ensemble-averaged velocity vector pattern, which identifies the large-scale coherent structures. The iso-contour lines in this figure represent values equal to 10%, 20%, 30%, 40%, 50%, 60%, 70%, 80%, 90%, and 95% of the peak values. The white regions in the figure relate to values of the indicator function that are effectively zero and represents the free-stream fluid. The dark zones correspond to the highest levels of the function. This represents the most intense turbulence activity. The grey regions with velocity vectors pointing towards the inside of the wake correspond to the areas where the free-stream fluid is pulled towards the turbulent core region of the flow by the structures as the fine-activity intensifies. The means by which the originally irrotational free-stream fluid is 'absorbed' into the weak flow and subsequently acquires turbulent vorticity is essentially the entrainment process, and we refer to this type of plot as an 'entrainment map' of the flow.

It can be seen from these figures that although the fine-scale turbulent activity is essentially random, the distribution of this activity in the flow is highly dependent upon the presence of large-scale coherent structures. The most intense fine-scale turbulence activity is, in fact, concentrated near the cores of the coherent structures.

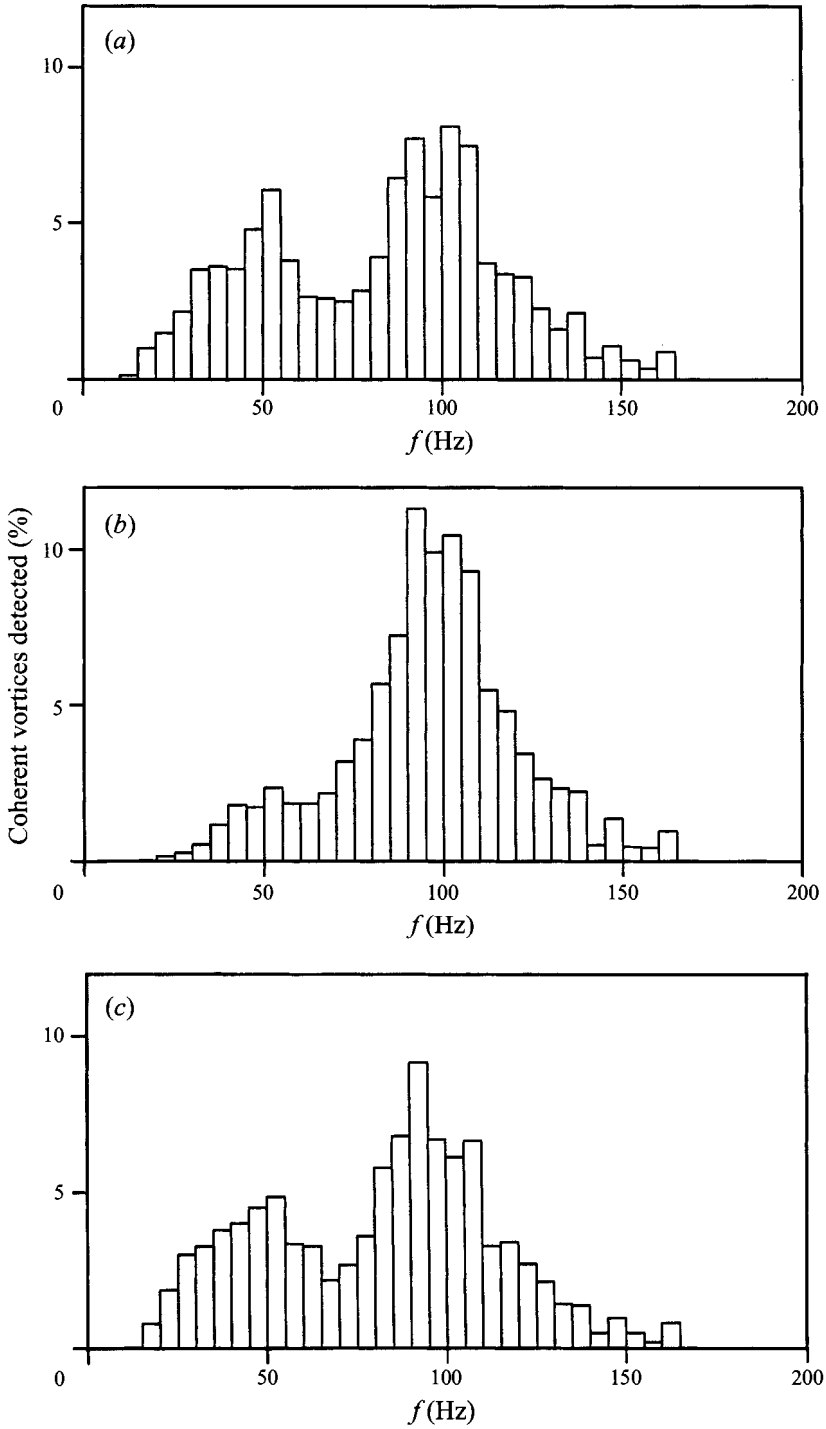


FIGURE 7(a-c). For caption see facing page.

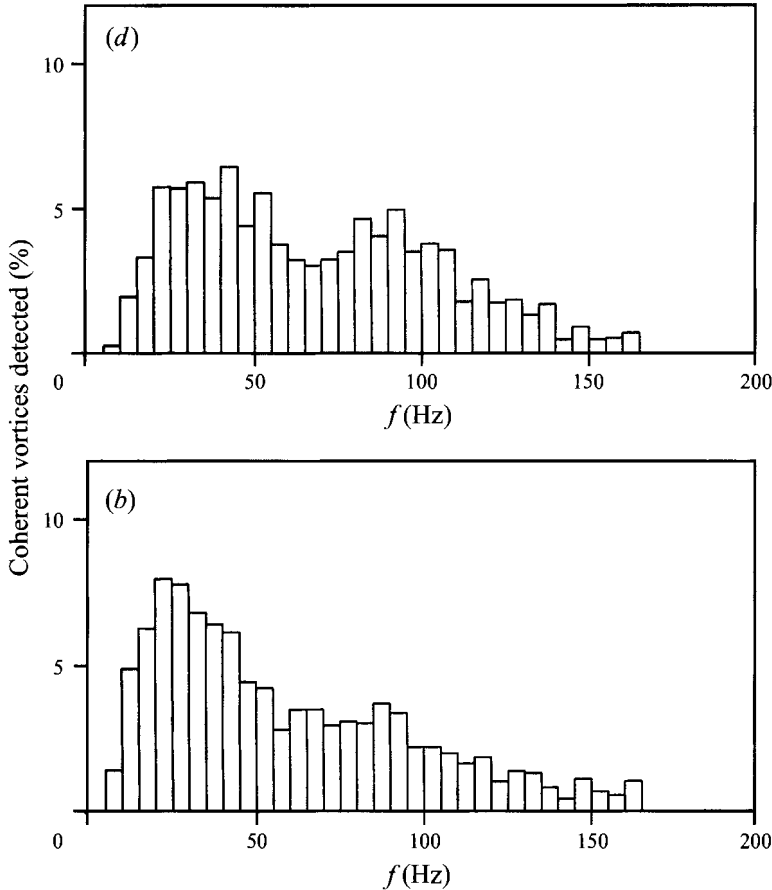


FIGURE 7. Histograms of the detection frequencies of the spanwise structures. (a) $x/d = 20$, (b) $x/d = 24$, (c) $x/d = 50$, (d) $x/d = 75$, (e) $x/d = 100$.

3.3. Some statistical properties of the spanwise structures

Figure 6 shows the streamwise variation of the number of realizations detected by the pattern-recognition analysis for the spanwise and lateral structures (the data for the lateral structures will be dealt with in the next section). In this figure, N is the number of realizations in the ensemble-average and represents the number of structures (within a specific time interval) at different stages in the development of the flow. The data are normalized by the predicted number of vortices based on the measured characteristic frequency at $24d$. At this station, the number of realizations (about 3500) detected was a maximum. These realizations account for about 88% of the predicted vortices. Upstream of $24d$, in the formation region, small-scale vortices merge to form large-scale coherent motions (Huang & Keffer 1996). Downstream of $24d$, the number of realizations decreases gradually, indicating that progressively fewer coherent structures are identified. At $100d$, the number is about 50% of the original number detected in the near wake.

The histograms of the detection frequencies are shown in figure 7, for the streamwise locations of $20d$, $24d$, $50d$, $75d$ and $100d$ respectively. This figure provides a statistical indication of how frequently the coherent spanwise structures occur at specific x -locations. The vertical coordinate in the figure is the percentage of coherent structures which occur at each frequency interval. These data were obtained on the basis of the

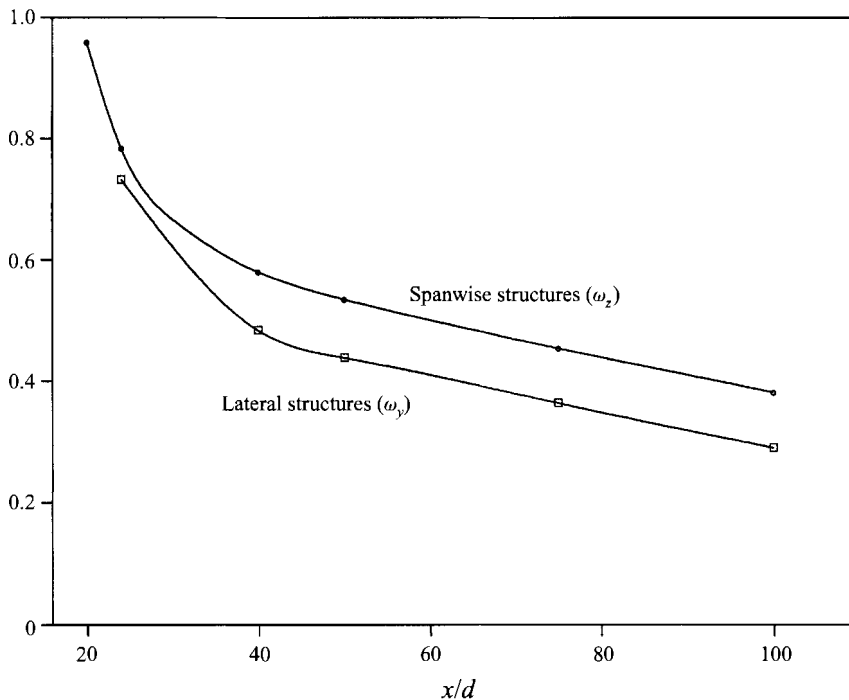


FIGURE 8. Streamwise variation of peak coherent vortices.

statistical analysis of $1/\Delta\tau$, where $\Delta\tau = \tau(m) - \tau(m-1)$, $m = 1, m_x$ and $\tau(m)$ is the time when a structure is identified within the signal. At $20d$, these vortices are detected mostly at both the characteristic frequency and its sub-harmonic frequency, i.e. the histogram is bimodal. At this location, there is no prominent peak occurring at the sub-harmonic frequency in the u - and v -velocity spectra. At $24d$, where the periodicity in the velocity signals is most prominent, the histogram is concentrated around the characteristic frequency of about 100 Hz. This implies that the coherent vortices have a significant periodicity. From figures 7(a) and 7(b), we can judge that a few large-scale vortices are formed at $20d$, with a spacing corresponding to that of Kármán-like structures, while others, which are detected at $24d$, are still undergoing the merging process and are not selected by the pattern-recognition procedure (i.e. some merging vortices have not been identified as coherent structures yet). Downstream of $24d$, the spanwise structures gradually lose their periodicity, as would be expected in a dissipative flow.

For the purpose of evaluating the strength of the coherent structures in the wake flow, the peak coherent vorticity (maximum ω_z value) has been calculated from the ensemble-averaged u - and v -velocities. Figure 8 depicts the variation of this vorticity, which is seen to decrease as the flow moves from the near to the far region.

4. Evolution of lateral structures

Figure 9 shows a realization of u - and w -velocity vectors and the streamline patterns in a horizontal plane at $y/l_0 = -0.9$ and $x/d = 24$. In the centre of this figure, a pair of counter-rotating lateral vortices can be clearly identified. These patterns suggest that lateral coherent structures exist in the flow. In order to see whether this is so, and to

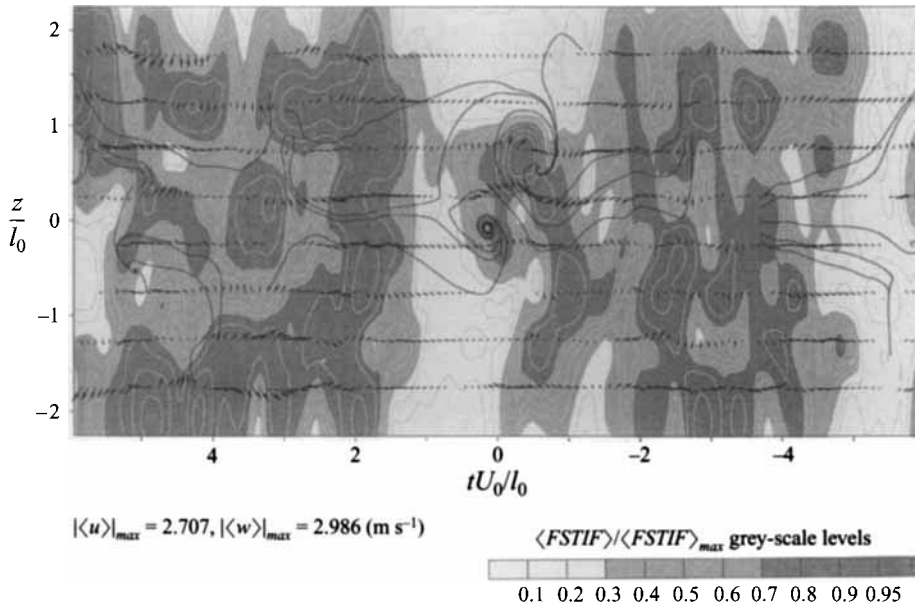


FIGURE 9. A typical realization of u - and w -velocities superimposed on the fine-scale indicator function contours, $x/d = 24$.

provide a statistical description of these lateral structures, pattern-recognition analysis was performed on the u - and w -velocity data measured in several horizontal planes at different streamwise locations. The initial template for this analysis is the vortex pattern (similar to figure 2) used in the eduction of the spanwise structures discussed earlier.

4.1. Ensemble-averaged velocities

Figure 10(a) shows the ensemble-averaged u - and w -velocity vectors at $x = 24d$. The corresponding vorticity iso-contours are shown in figure 10(b). The vector plot (figure 10a) displays a counter-clockwise rotational pattern in the centre. This is evidence that lateral structures do exist at this streamwise position. Although the vector plot does not give a clear indication of any other rotation, the vorticity plot (figure 10b) contains a negative contour on the upper side of central positive contours. From this, it can be speculated that the lateral vortices have a tendency to occur in the form of counter-rotating pairs. Moreover, the distance between two simultaneously occurring vortices is not fixed. Notice that the vector plot also exhibits a pattern of alternate forward and backward velocities in the regions before and after the central structure. The implication here is that the lateral structures are closely related to the spanwise structures. It may be remarked that, with the velocity results shown in figure 10(a) used as a template, the iterative pattern-recognition analysis yields an ensemble-averaged pattern dominated by the strong forward and backward velocities, indicating that the spanwise structures are the dominant mechanism for the u - and w -fluctuations. These are therefore more significant than the lateral structures at this streamwise location. (Figure 10(a) shows the velocity pattern for those cases where lateral structures are present. The prominent mode of the coherent motions, however, is that due to the spanwise structures.)

At $x = 50d$, i.e. in the intermediate region of the wake, the ensemble-averaged velocity pattern obtained after one iteration (via the single-vortex template) is similar

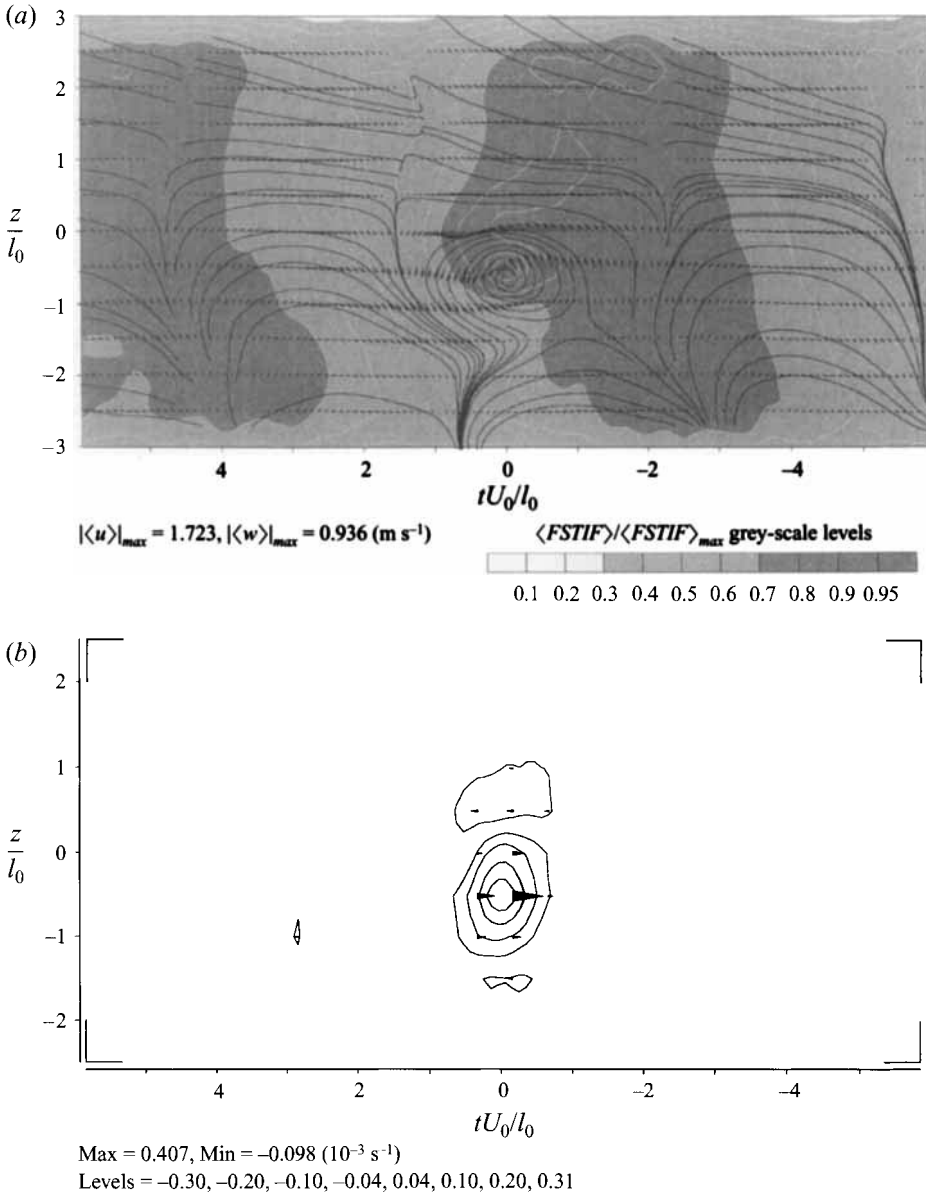


FIGURE 10. (a) Ensemble-averaged u - and w -velocity vectors in the near region, superimposed on the grey-scaled iso-contours of the fine-scale indicator function, $x/d = 24$, $y/l_0 = -0.9$. (b) Iso-contours of lateral ω_y -vorticity corresponding to (a).

to that shown in figure 10(a), except that the alternate pattern of forward-backward velocities becomes very weak in the regions before and after the central structure. Furthermore, unlike the results for the near region, the rotational pattern in the centre is still present after several iterations. This structure is believed to be the dominate and representative pattern in the horizontal plane. Figure 11(a) is the ensemble-averaged velocity pattern obtained after five iterations. In this figure, a counter-clockwise rotation can be identified, which represents an ensemble of counter-clockwise vortices educed on the basis of the original single-vortex template. In addition, the pattern-recognition technique also detects, on the upper side of the figure, another vortex

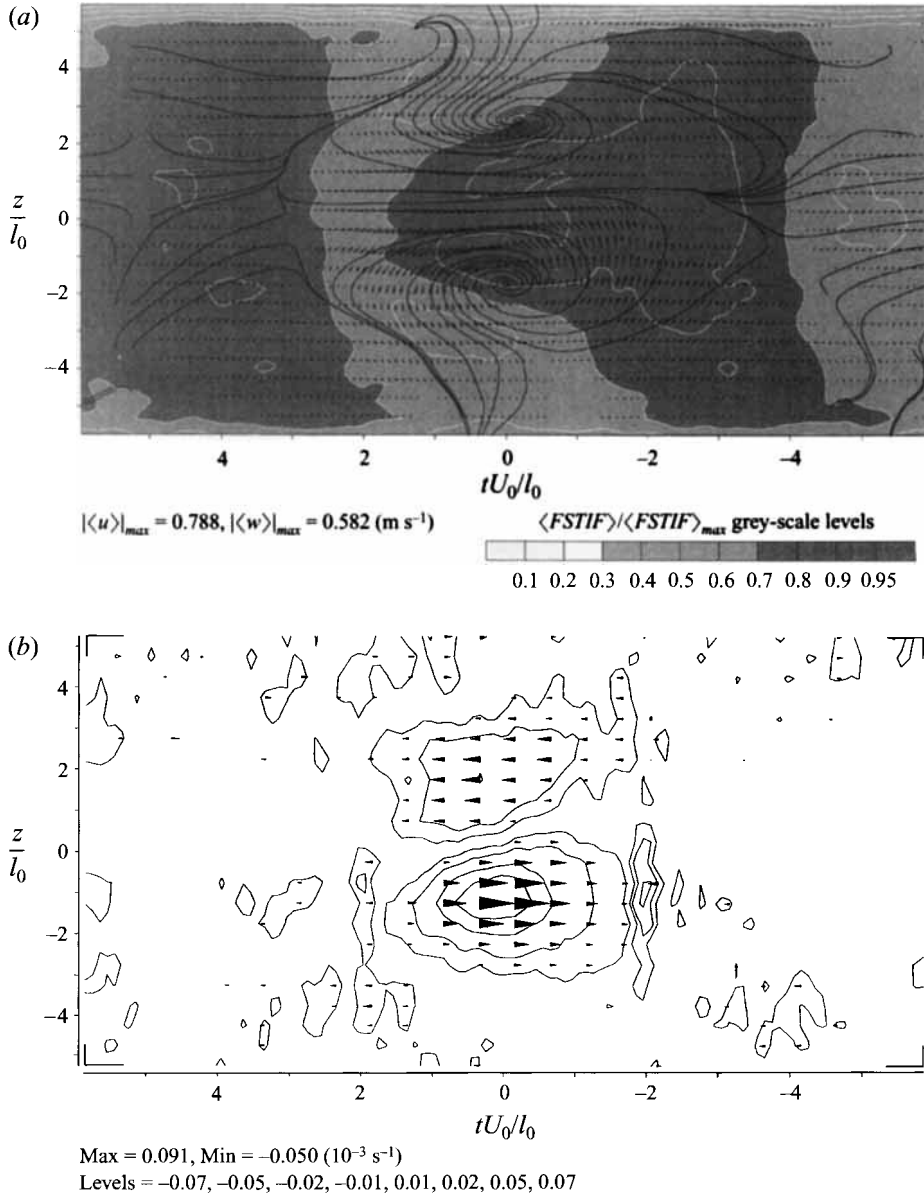


FIGURE 11. (a) Ensemble-averaged u - and w -velocity vectors in the intermediate region, superimposed on the grey-scaled iso-contours of the fine-scale indicator function, $x/d = 50$, $y/l_0 = -1.2$. (b) Iso-contours of lateral ω_y -vorticity corresponding to (a).

pattern with clockwise rotation. Since this ‘extra’ rotation is not present in the initial template, it can be inferred that a significant number of clockwise vortices occur simultaneously with the counter-clockwise vortices. The iso-contours of the corresponding vorticity are presented in figure 11(b). These results establish that, on average, the lateral structures (rollers) do not occur in isolation at this streamwise location. Rather, they occur in pairs, i.e. in the form of double rollers, with a backward flow between them.

The plot of ensemble-averaged velocities after five iterations at $x/d = 100$ (figure 12a) also shows a double-roller structure in the horizontal plane, similar to figure 11(a)

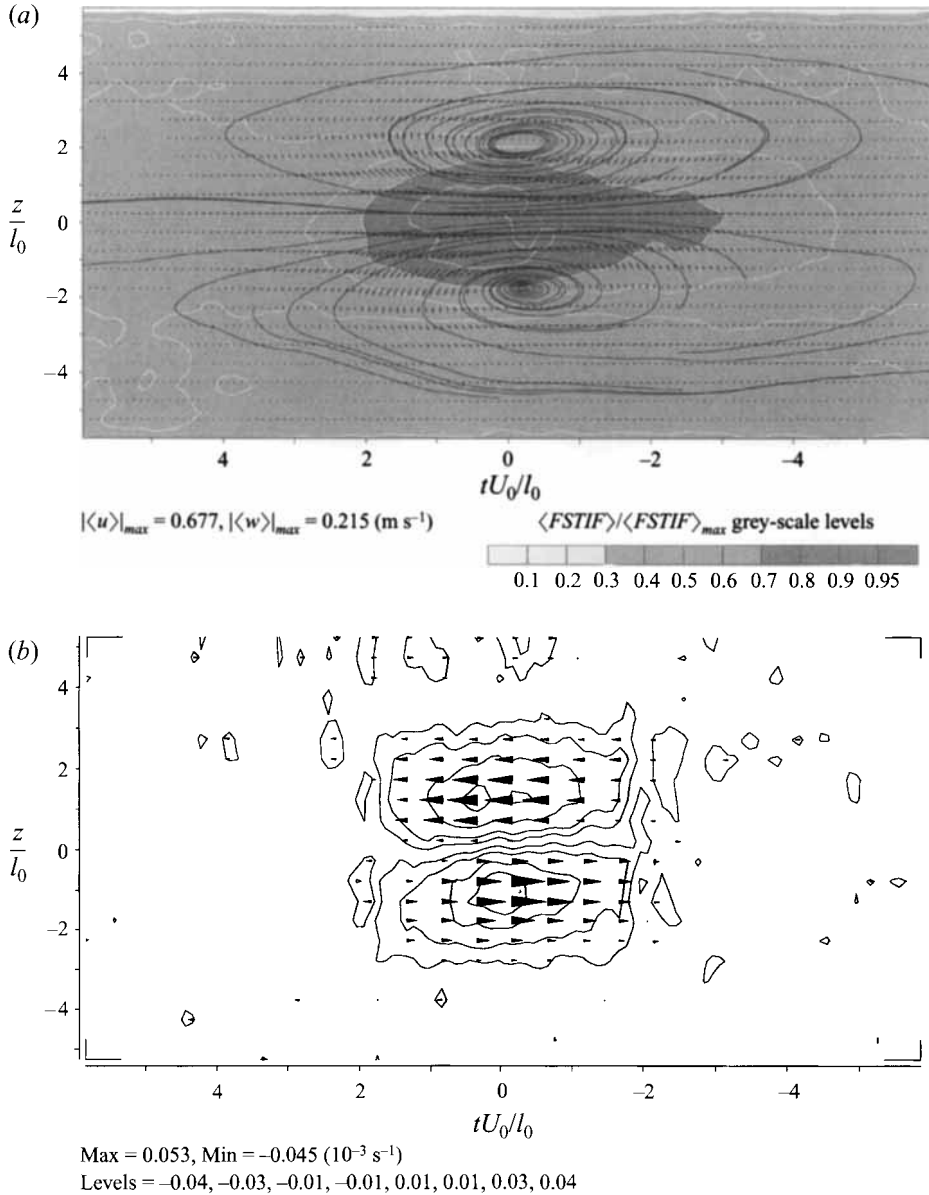


FIGURE 12. (a) Ensemble-averaged u - and w -velocity vectors in the far region, superimposed on the grey-scaled iso-contours of the fine-scale indicator function, $x/d = 100$, $y/l_0 = -2$. (b) Iso-contours of lateral ω_y -vorticity corresponding to (a).

in the intermediate region. The corresponding vorticity iso-contours are displayed in figure 12(b). In this figure, the vorticity relating to the clockwise rotation (negative ω_y) is very close to that of the counter-clockwise rotation (positive ω_y). Thus, the lateral structure pairs become more prominent as they move further downstream.

4.2. Some statistical properties of the lateral structures

The streamwise variation of the number of realizations detected and the coherent peak vorticity (ω_y) for the lateral structures, i.e. the single rollers, are presented in figures 6 and 8, respectively. The number of realizations detected by the pattern-recognition

analysis remains almost unchanged within the region investigated in the present study. There is only a slight increase prior to $50d$ and a slight decrease beyond this location. Thus, we infer that the lateral structures detected at different streamwise locations probably represent the same group of vortices (the observer would be travelling with the structures). In other words, these vortices do not merge, nor do they decay significantly. However, they do undergo a gradual diffusion, since the peak coherent vorticity decreases and the size of the structures increases. As can be seen from figure 8, the peak vorticity (ω_y) for the lateral structures decreases in a similar fashion as for the spanwise structures. It is interesting to note that, although the level of the lateral vorticity is smaller than that of the spanwise vorticity at the same streamwise position, the magnitudes are comparable. Moreover, it can be interpreted that the lateral and the spanwise coherent structures are roughly of equal strength in the near region, and they decay at almost the same rate as the flow moves downstream.

5. Relationship between spanwise and lateral structures

There are two main issues with respect to the relationship between spanwise and lateral coherent structures. First, although it is known that the two structures occur quite repetitively in wake flows, it is still not clear whether they occur simultaneously (i.e. do they have a definite phase relation with each other?). Secondly, on the assumption that the two structures occur simultaneously, it is still not clear how the structures are connected topologically. It is noted that, with respect to the lateral structures, the characteristic vorticity, ω_y , can be attributed to either ‘ribs’ or ‘legs’, as pointed by Hayakawa & Hussain (1989), and, therefore, one must discriminate between them. We try to resolve these issues in a definitive manner, using a statistical approach involving ensemble-averages.

5.1. Identification of spanwise structures in horizontal planes

As can be seen from the velocity vector and streamline patterns in figure 9, which is an ‘instantaneous’ entrainment map for a horizontal plane at $24d$, there is a pair of counter-rotating lateral vortices in the centre of the figure. The fine-scale indicator in this figure shows zones of alternate dark and light colours in the streamwise direction. Based on the entrainment map for the vertical plane at the same streamwise location (figure 3*a*), the cores of the spanwise Kármán-like structures are slightly closer to the downstream interfaces of the dark regions. We infer therefore, from figure 9, that two spanwise vortices exist in the plane, with the cores located at $tU_0/l_0 \approx -3.5$ and $\approx +3.0$. From the superimposed streamline and the grey-scale patterns of the fine-scale indicator function, it can be concluded that the two lateral vortices in the centre of figure 9 are located between the cores of the two spanwise structures and closer to the upstream interface of the structure centred around $tU_0/l_0 \approx -3.5$. In other words, they are most likely the ribs (Hayakawa & Hussain 1989) in the flow.

5.2. Connections between two structures in different regions of the wake

Although figure 9 provides a very vivid example of the rib structures and their relationship with the spanwise vortices, it represents only a single realization of the lateral structures. Figure 10(*a*) is the corresponding ensemble-averaged entrainment map for the lateral structures at the streamwise position of $24d$. This figure displays the same basic features as figure 9, except that the iso-contours are much smoother. This signifies that, in the near-wake region, the lateral structures do not occur randomly. Rather they occur close to the upstream side of the spanwise Kármán-like structures.



FIGURE 13. Conceptual picture of ribs and spanwise eddies in the near wake.

Thus, the two types of structures are connected, and the lateral structures are the ribs. Figure 13 shows a conceptual sketch of the rib structures and their connection with the spanwise structures. In this sketch, the curved surfaces represent the turbulent/non-turbulent interface. The cylinders correspond to the spanwise structures and the filaments depict the lateral rib structures.

The entrainment map for an intermediate location in the flow, namely $x = 50d$, is depicted in figure 11(a). Clearly, the regions of intense turbulence activity (dark shades) do not extend throughout the entire range of the figure in the spanwise direction. Since the distribution of fine-scale activity is contingent upon the shape of the coherent structures, a significant spanwise variation of the ensemble-averaged fine-scale indicator function (within a given horizontal plane) implies that the centrelines of the spanwise vortices are curved, i.e. these vortices are three-dimensional. In addition, it is evident that the centres of the lateral structures are still located on the upstream sides of the spanwise vortices, i.e. the lateral structures are rib structures in the intermediate region.

As can be seen from figure 13, the regions of relatively calm fine-scale turbulence activity (light shades) are located at $tU_0/l_0 \approx +0.5$ and $z/l_0 \approx \pm 3$, on the two sides of the lateral structures in the centre, and at $tU_0/l_0 \approx -5.0$, along the downstream side of the spanwise structures. In other words, because of the rib structures (counter-rotating vortices) in the centre of the figure, free-stream fluid is pulled in on the two sides of these vortices, while the intensity of the fine-scale turbulence activity is still relatively high in the central region between the two vortices. Since these rib structures will interact with the spanwise vortices, the velocity induced by the former will cause the axes of the latter to bend. We conclude therefore, that the occurrence of the rib structures is responsible for the three-dimensionality of the large-scale spanwise vortices.

Based on the results from the intermediate region, a sketch portraying the relationship between the lateral and spanwise structures is given in figure 14. In this figure, the lateral structures are assumed to occur as a pair of counter-rotating vortices, and the flow is considered to be symmetrical with respect to the vertical centreplane associated with the coherent structures in the flow, i.e. where the spanwise coherent vorticity is maximum. The interaction between the ribs and the spanwise vortex induces a downward motion in the outer part of the latter, resulting in the formation of 'legs'. Moreover, the ribs and legs tend to be intertwined.

The entrainment map in the horizontal plane at $x = 100d$ is shown in figure 12(a), for the (double-roller) lateral structures in the far wake. In this figure, the region of intense turbulence activity (dark shades) is isolated in the centre, indicating that the far-wake coherent structures are more three-dimensional (with smaller spanwise dimension) than those in the intermediate wake. Furthermore, the location of the

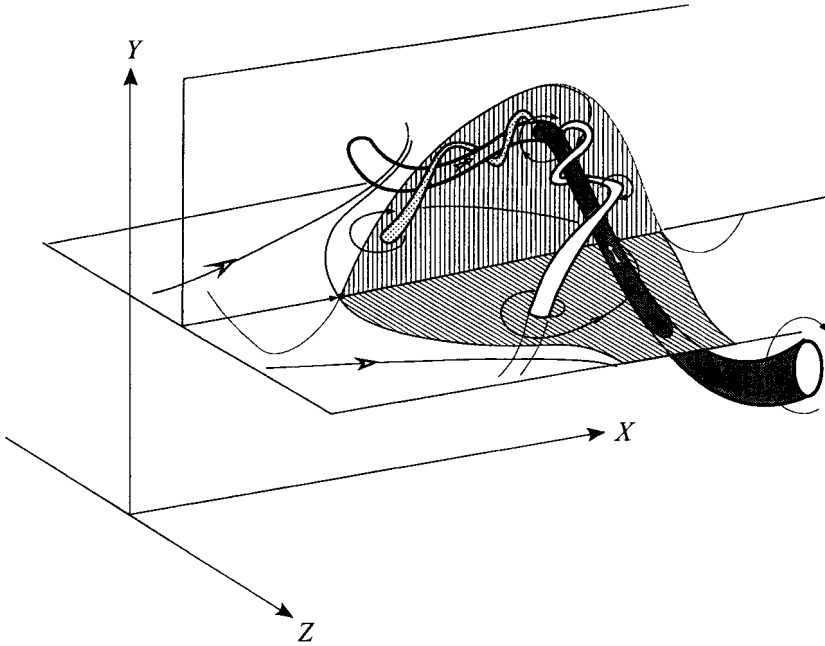


FIGURE 14. Conceptual picture of the interaction between ribs and spanwise structures in the intermediate region.

centre of rotation associated with the lateral structures is close to the location where the maximum fine-scale turbulence occurs. There is no difference between the streamwise positions of these two locations. Thus is the far-wake region, the lateral and the spanwise vortices occur simultaneously, without a phase lag. Figure 12(a) also shows that the high value of fine-scale indicator function is concentrated in the centre of the figure. In other words, the cores of the coherent structures (spanwise and lateral) are both included in a bulge of turbulent fluid with limited extent in both the streamwise and spanwise directions. We conclude, therefore, that the original two-dimensional spanwise structures become three-dimensional in the far wake and the dominant lateral structures in the far wake are the legs of these structures. The rib structure, which, in the near and intermediate regions ($x \leq 50d$), are separate entities distinct from the original spanwise structures, now intertwine and merge with the legs in the far wake. At this stage, the coherent structures are likely to have evolved into single entities: hairpin-like three-dimensional vortices.

6. Concluding remarks

The present results indicate that the coherent ω_y vorticity can be attributed to either 'ribs' or 'legs' depending on the different stages of evolution of the wake flow. Between the streamwise positions of $20d$ and $50d$, these vortices are the ribs which are connected to the spanwise vortices but with a certain phase lag with the latter. As the flow moves from the near to the far regions, the original spanwise structures undergo a three-dimensional deformation. Somewhere beyond $50d$, these ribs become an integral part of the three-dimensional coherent structures, i.e. evolve into legs.

In summary, the present porous-body wake is seen to exhibit an interesting life-cycle of vortex structures. It starts with random and small-scale eddies in the formation

region immediately behind the mesh. These subsequently merge into well-organized large-scale spanwise structures. Eventually, as the structures are convected downstream, turbulent diffusion takes over and they lose their coherence.

This research was supported by the Natural Sciences and Engineering Research Council of Canada through Grant A-2746.

REFERENCES

- ANTONIA, R. A., BROWNE, L. W. B., BISSET, D. K. & FULACHIER, L. 1987 A description of the organized motion in the turbulent far wake of a cylinder at low Reynolds number. *J. Fluid Mech.* **184**, 423–444.
- CIMBALA, J. M., NAGIB, H. M. & ROSHKO, A. 1988 Large structure in the far wakes of two-dimensional bluff bodies. *J. Fluid Mech.* **190**, 265–298.
- FERRÉ, J. A. & GIRALT, F. 1989 Pattern-recognition analysis of the velocity field in plane turbulent wakes. *J. Fluid Mech.* **198**, 27–64.
- FERRÉ, J. A., MUMFORD, J. C., SAVILL, A. M. & GIRALT, F. 1990 Three-dimensional large-eddy motions and fine-scale activity in a plane turbulent wake. *J. Fluid Mech.* **210**, 371–414.
- GIRALT, F. & FERRÉ, J. A. 1993 Structure and flow patterns in turbulent wakes. *Phys. Fluids A* **5**, 1783–1789.
- HAYAKAWA, M. & HUSSAIN, A. K. M. F. 1989 Three-dimensionality of organized structures in a plane turbulent wake. *J. Fluid Mech.* **206**, 375–404.
- HUANG, Z. & KEFFER, J. F. 1996 Development of structures within the turbulent wake of a porous-body. Part 1. The initial formation region. *J. Fluid Mech.* **329**, 103–115.
- ZHOU, Y. & ANTONIA, R. A. 1993 A study of flow properties near critical points. In *Eddy Structure Identification in Free Turbulent Shear Flows* (ed. J. P. Bonnet & M. Glauser), pp. 137–149. Kluwer.